



Radio-detection of neutrino-induced air showers: the influence of topography

V. Decoene, N. Renault-Tinacci, O. Martineau-Huynh, Didier Charrier, K. Kotera, S. Le Coz, V. Niess, M. Tueros, A. Zilles

► To cite this version:

V. Decoene, N. Renault-Tinacci, O. Martineau-Huynh, Didier Charrier, K. Kotera, et al.. Radio-detection of neutrino-induced air showers: the influence of topography. Nucl.Instrum.Meth.A, 2021, 986, pp.164803. 10.1016/j.nima.2020.164803 . hal-02101669

HAL Id: hal-02101669

<https://hal.science/hal-02101669>

Submitted on 24 Oct 2022

HAL is a multi-disciplinary open access archive for the deposit and dissemination of scientific research documents, whether they are published or not. The documents may come from teaching and research institutions in France or abroad, or from public or private research centers.

L'archive ouverte pluridisciplinaire **HAL**, est destinée au dépôt et à la diffusion de documents scientifiques de niveau recherche, publiés ou non, émanant des établissements d'enseignement et de recherche français ou étrangers, des laboratoires publics ou privés.



Distributed under a Creative Commons Attribution - NonCommercial 4.0 International License

Radio-detection of neutrino-induced air showers: the influence of topography

V. Decoene^a, N. Renault-Tinacci^a, O. Martineau-Huynh^{b,c,a}, D. Charrier^d,
K. Kotera^a, S. Le Coz^c, V. Niess^e, M. Tueros^{f,a}, A. Zilles^a

^a*Sorbonne Université, CNRS, UMR 7095, Institut d'Astrophysique de Paris, 98 bis bd
Arago, 75014 Paris, France*

^b*Sorbonne Université, Université Paris Diderot, Sorbonne Paris Cité, CNRS/IN2P3,
LPNHE, Paris, France*

^c*National Astronomical Observatories of China, Chinese Academy of Science, Beijing
100012, P.R. China*

^d*Université de Nantes, IMT-Atlantique, CNRS/IN2P3, SUBATECH, Nantes, France*

^e*Université Clermont Auvergne, CNRS/IN2P3, LPC, Clermont-Ferrand, France*

^f*Instituto de Física La Plata - CONICET, Argentina*

Abstract

Neutrinos of astrophysical origin could be detected through the electromagnetic radiation of the particle showers induced in the atmosphere by their interaction in the Earth. This applies in particular for tau neutrinos of energies $E > 10^{16}$ eV following Earth-skimming trajectories. The $\sim 1^\circ$ beaming of the radio emission in the forward direction however implies that the radio signal will likely fly above a detector deployed over a flat site and would therefore not be detected.

We study here how a non-flat detector topography can improve the detection probability of these neutrino-induced air showers. We do this by computing with three distinct tools the neutrino detection efficiency for a radio array deployed over a toy-model mountainous terrain, also taking into account experimental and topographic constraints. We show in particular that ground topographies inclined by few degrees only induce detection efficiencies typically three times larger than those obtained for flat areas [for favorable trajectories](#). We conclude that the topography of the area where the detector is deployed will be a key factor for an experiment like GRAND.

Keywords: ultra-high-energy cosmic-rays, ultra-high-energy neutrinos, radio-detection, air-showers.

Email address: decoene@iap.fr (V. Decoene)
Preprint submitted to Elsevier

October 7, 2020

1. Introduction

Ultra high energy neutrinos (UHE ν) are valuable messengers of violent phenomena in the Universe ([1, 2] and references therein). Their low interaction probability with matter allows them to carry unaltered information from sources located at cosmological distances, but, on the other hand, makes their detection challenging: non-negligible detection probability can be achieved only with large volumes of dense targets.

At neutrino energies targeted here ($E > 10^{16}$ eV), the Earth is opaque to neutrinos. Therefore only Earth-skimming trajectories yield significant probability of neutrino interaction with matter, leading to a subsequent tau decay in the atmosphere, eventually inducing an extensive air-shower (EAS). The detection of these EAS has been proposed as a possible technique to search for these cosmic particles [3]. The progress achieved by radio-detection of EAS in the last 15 years [4, 5, 6, 7, 8, 9] combined with the possibility to deploy these cheap, robust detectors over large areas open the possibility to instrument giant radio arrays designed to hunt for neutrino-induced EAS as proposed by the GRAND project [2, 10].

An EAS emits a radio signal via two well understood mechanisms : the *Askaryan effect* [11, 12] and the *geomagnetic effect* [13, 14], which add up coherently to form detectable signals in the frequency range between tens to hundreds of MHz. The interplay between these two effects induces an azimuthal asymmetry of the electric field amplitude along the shower axis [15, 16].

The nearly perfect transparency of the atmosphere to radio waves, combined with the strong relativistic beaming of the radio emission in the forward direction [17] make it possible to detect radio signals from air showers at very large distances from their maximum of development X_{\max} : a 2×10^{19} eV shower was for example detected by the Auger radio array with a X_{\max} position reconstructed beyond 100 km from shower core [18]. This is obviously an important asset in favor of radio-detection of neutrino-induced air showers.

The strong beaming of the radio signal also implies that the topography of the ground surface may play a key role in the detection probability of the induced EAS. The primary objective of this article is to perform a quantitative study of the effects of ground elevation on the detection probability of neutrino-induced air showers. To do this, we use a toy configuration where a radio array is deployed over a simplified, generic topography. We compute the response of this setup to neutrino-induced showers with three

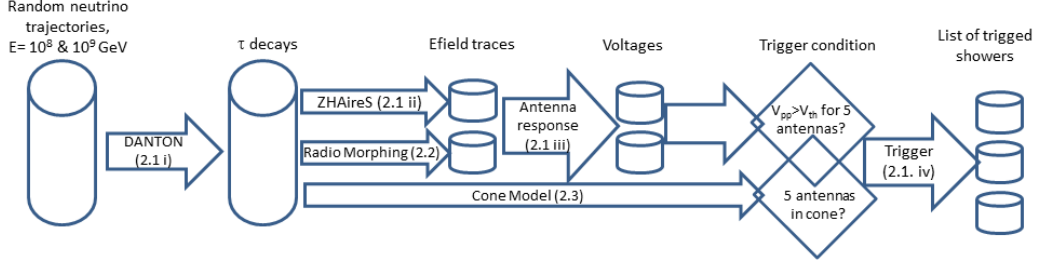


Figure 1: General structure of the three simulation chains (*microscopic*, *Radio Morphing* and *Cone* models) used in this study. The sections where their various elements are described are indicated in parenthesis. The trigger condition for the *microscopic* and *Radio Morphing* methods is fulfilled if five antennas or more with peak-peak voltages larger than a threshold value V_{th} set to 5 times (conservative) or twice the minimal background noise level. For the *Cone model*, the trigger condition is fulfilled if five antennas or more are within the volume of the cone modeling the shower radio emission.

different simulation chains, ranging from a fast and simple estimation using a parametrization of the expected signal amplitude, to a detailed and time consuming Monte-Carlo. This is motivated by the fact that full Monte-Carlo tools are CPU-intensive treatments, to the point of becoming prohibitive when it comes to simulating radio detection by large antenna arrays. The secondary purpose of this paper is therefore to determine if reliable results can be obtained with faster treatments than full Monte-Carlo simulation codes.

In section 2 we present the general principle of our study, in section 3 we detail the implementation of the three simulation chains used, and finally in section 4 we discuss the results.

2. General principle

Three simulation chains are used in this study. Their general principles are presented in sections 2.1 to 2.3, and summarized in Figure 1. In section 2.4, we present the toy detector configuration used for the study.

2.1. End-to-end microscopic simulation

The first simulation chain consists of four independent steps:

- (i) We produce a fixed number of tau decays induced by cosmic tau-neutrinos (ν_τ) interacting in a spherical Earth. This is done for two neutrino energies ($E_\nu = 10^9$ and 10^{10} GeV) with a dedicated Monte-Carlo engine: DANTON [19, 20], further described in section 3.1.
- (ii) We compute the electromagnetic field induced at the location of the detection units by the showers generated by these tau decays. This is done through a full *microscopic simulation* of the particles in the EAS and of the associated electromagnetic radiation using the ZHAireS [21] simulation code (see section 3.2.1 for details).
- (iii) The voltage induced by the radio wave at the antenna output is then computed using a modelling of the GRAND HORIZON ANTENNA [2] performed with the NEC4 [22] code. This is detailed in section 3.3.
- (iv) If the peak-to-peak amplitude of the output voltage exceeds the defined threshold for five antennas or more, then the neutrino is considered as detected (see section 3.4 for more details). This threshold value is either twice (aggressive scenario) or five times the minimal noise level (conservative scenario).

2.2. Radio-Morphing

Monte-Carlo simulations of the electric field provide the most reliable estimate of the detection probability of a shower, and are therefore used as a benchmark in this work. They however require significant computational resources: the CPU time is mainly proportional to the number of simulated antennas and can last with ZHAireS up to ≈ 72 h on one core for 1000 antennas given our simulation parameters.

An alternative simulation chain therefore uses the so-called *Radio Morphing* method [23] instead of ZHAireS for the electric field computation. *Radio Morphing* performs a very fast, semi-analytical computation of the electric field (see section 3.2.2 for details). The antenna response and the trigger computation are simulated in the same way as for the *microscopic simulation* chain. The gain in computation times allows to study a larger number of configurations than with the *microscopic* approach.

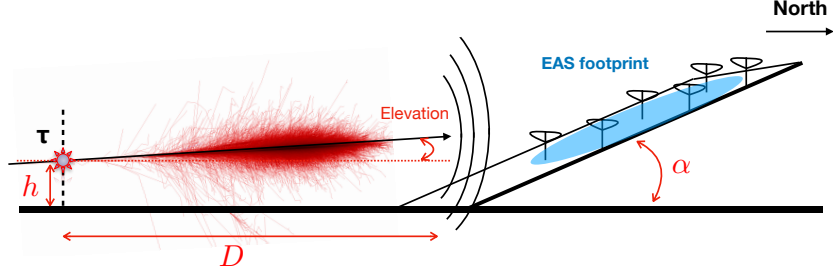


Figure 2: Layout of the toy-setup considered in this study. A tau particle decays at a location represented as a star, producing an air shower. The radio signal emitted by the shower impinges the detector plane, tilted by an angle α from the horizontal. The intersection between the detector plane and the horizontal plane is set at a horizontal distance D from the decay point. The parameter D is therefore a measurement of the amount of free space in front of the detector.

109 2.3. Cone Model

110 Even if significantly faster than the microscopic method, the *Radio Mor-*
 111 *phing* treatment still requires that the antenna response is computed, and
 112 thus implies that hundreds of time traces for electric field and voltage need
 113 to be handled for each simulated event. A third, much lighter method is
 114 therefore used in this study. It is based on a geometric modeling of the
 115 volume inside which the electromagnetic field amplitude is large enough to
 116 trigger an antenna. We give to this volume the shape of a cone, oriented
 117 along the shower axis, with its apex placed at the X_{\max} position, half-angle
 118 Ω and height H . Values of Ω and H depend on shower energy, and are ad-
 119 justed from ZHAireS simulations (see section 3.5 for details). A shower is
 120 considered as detected if at least five antennas are within the cone volume.
 121 A similar *Cone Model* was used to compute the initial neutrino sensitivity
 122 of the GRAND detector [24]. Being purely analytical, this method produces
 123 results nearly instantaneously and requires only minimal disk space and no
 124 specific simulation software, an attractive feature when it comes to perform
 125 simulation for thousands of detection units covering vast detection areas.

126

127 2.4. Toy detector configuration

128 The detector considered in this study is presented in Figure 2. It is a
 129 rectangular grid with a step size of 1000 m between neighbouring antennas.
 130 This large step size is a distinct feature of the envisioned dedicated radio array

131 for the detection of neutrino-induced air showers [17]. It is a compromise
 132 between the need for very large detection areas imposed by the very low event
 133 rates expected for one part, and the instrumental and financial constraints
 134 which limit the number of detection units for the other.

135 In our study we use a simplified, toy setup configuration where the an-
 136 tenna array is deployed over a plane inclined by an adjustable angle α (also
 137 called "slope" in the following) with respect to an horizontal plane. We
 138 restrict our treatment to showers propagating to the North, i.e. directly to-
 139 wards the detector plane. For other directions of propagation, the size of
 140 the shower footprint on ground —hence its detection probability— would
 141 directly depend on the width of the detector plane. Defining a specific value
 142 for this parameter would be highly arbitrary, given the great diversity of to-
 143 pographies existing in reality. For showers propagating towards the detector
 144 however, the shower footprint is aligned with the detector longitudinal axis
 145 (see Figure 2), and the detector width then has a negligible effect on the
 146 shower detection efficiency. This motivates our choice to restrict ourselves to
 147 this single direction of propagation. The horizontal distance between the tau
 148 decay point and the foot of the detector, D , can be understood as the amount
 149 of empty space in front of the detector over which the shower can develop and
 150 the radio signal propagate. It is therefore closely related to the topography
 151 of the detection site. The reference ground elevation is chosen to be 1500 m
 152 above sea level (a.s.l.). A maximum altitude of 4500 m a.s.l. is set for the
 153 antennas, as larger elevation differences are unrealistic. The vertical devia-
 154 tion due to Earth curvature can be estimated by $2\delta h \approx R_{\text{earth}}(L/R_{\text{earth}})^2$ km,
 155 where $L \ll R_{\text{earth}}$ is the longitudinal distance between the maximum devel-
 156 opment of the shower and the observer. For $L = 50$ km, we find $\delta h < 100$ m.
 157 A flat Earth surface is therefore assumed in this toy setup configuration.

158 The slope α and the distance D are the two adjustable parameters of the
 159 study. Values of α vary from 0 to 90° and D ranges between 20 and 100 km,
 160 covering a wide variety of configurations. As will be detailed in section 4.2,
 161 larger values of D are irrelevant because most showers would then fly over
 162 the detector (see Figure 12 in particular), an effect that would furthermore be
 163 amplified if the Earth curvature was taken into account. Values of α larger
 164 than 30° are also not realistic, because steeper slopes are not suitable to host
 165 a detector, but they are included in our study for the sake of completeness,
 166 and because these extreme cases will help us interpret the results of the study.

167 For each pair of values (α, D) , we process the two sets of tau decays of
 168 energies $E_\nu = 10^9$ GeV and $E_\nu = 10^{10}$ GeV with the three methods *micro-*

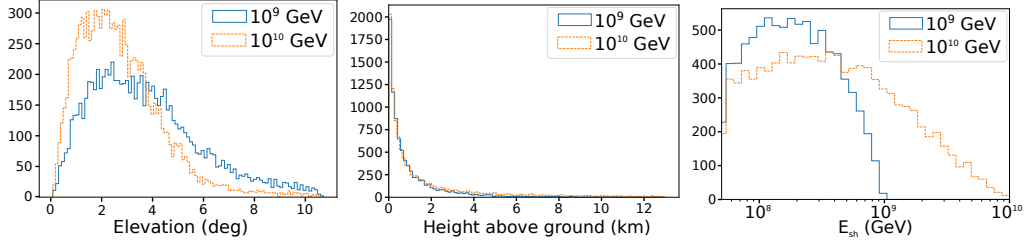


Figure 3: Distributions of tau decay elevation angles of particle trajectory measured with respect to a horizontal plane (*left*), height above ground at tau decay point (*center*) and shower energy (*right*) for the two sets of primary ν_τ energy considered in this study.

169 *scopic, Radio Morphing* and *Cone Model*. We then use the fraction of tau
 170 decays inducing a trigger by the detector to perform a relative comparison
 171 between (α, D) configurations. This treatment allows to directly assess the
 172 effect of topography on neutrino-induced shower detection efficiency —the
 173 purpose of this paper— for a reasonable amount of computing time, given
 174 the large number of configurations (α, D) considered in this study.

175

176 3. Computational methods

177 We present in the following the implementation of the methods described
 178 in sections 2.1 to 2.3.

179 3.1. Production of the shower progenitors

180 The production of the shower progenitors was performed with the DAN-
 181 TON software package [19, 20]. DANTON simulates interactions of tau neu-
 182 trinos and tau energy losses. It produces results compatible with similar
 183 codes [25]. Additionally DANTON offers the possibility to run simulations
 184 in backward mode (i.e. from tau decay upwards, with appropriate event
 185 weight computations), an attractive feature for massive simulations, and it
 186 also allows us to take into account the exact topography of the Earth sur-
 187 face [26]. It is however operated here in forward mode, i.e. as a classical
 188 Monte-Carlo. The primary neutrino source is set as mono-energetic and
 189 isotropic. A spherical Earth is used with a density profile given by the Pre-
 190 liminary Reference Earth Model (PREM) [27], but with the sea layer replaced
 191 by Standard Rock [28]. Two energy values are used for the primary neutrino
 192 flux: $E_\nu = 10^9$ GeV and 10^{10} GeV. The characteristics of the tau lepton

193 resulting from the interaction of the neutrino with the Earth and of all the
 194 particles produced during the decay of the tau in the atmosphere are also
 195 computed: decay position, list of products and their associated momenta.

196 For this study one million primary neutrinos were simulated per energy
 197 value. Those inducing tau decays in the atmosphere were then selected if the
 198 subsequent showers had energies above 5×10^7 GeV, because lower energies
 199 can hardly lead to detection for such a sparse array [5, 15]. In Figure 3, we
 200 show the distribution in energy, elevation angle and height of the two sets
 201 of tau decays. Among the surviving set, 100 were randomly chosen for each
 202 energy. This value is a good compromise between computation time and
 203 statistical relevance.

204 3.2. Simulation of the electric field

205 3.2.1. Microscopic method

206 In the *microscopic* method, the extensive air showers initiated by the by-
 207 products of the tau decay, and the impulsive electric field induced at the
 208 antenna locations were simulated using the ZHAireS software [21], an imple-
 209 mentation of the ZHS formalism [29] in the AIRES [30] cascade simulation
 210 software. To allow for geometries where cascades are up-going and initiated
 211 by multiple decay products, we implemented a dedicated module called RAS-
 212 PASS (Radio Aires Special Primary for Atmospheric Skimming Showers) in
 213 the ZHAireS software.

214 3.2.2. Radio Morphing

215 *Radio Morphing* [23] is a semi-analytical method for a fast computation of
 216 the expected radio signal emitted by an air shower. The method consists in
 217 computing the radio signal of any *target* air shower at any target position by
 218 simple mathematical operations applied to a single *generic* reference shower.
 219 The principle is the following:

- 220 i) The electromagnetic radiation associated with the *generic* shower is sim-
 221 ulated using standard microscopic tools at positions forming a 3D mesh.
- 222 ii) For each *target* shower, the simulated signals are scaled by numerical
 223 factors which values depend analytically on the energy and geometry of
 224 the *target* and *generic* showers.
- 225 iii) The *generic* 3D mesh is oriented along the direction of propagation of
 226 the target shower.

227 iv) The electromagnetic radiation expected at a given *target* position is com-
 228 puted by interpolation of the signals from the neighbouring positions of
 229 this 3-D mesh.

230 This technique lowers the required CPU time of at least two orders of magni-
 231 tude compared to a standard simulation tool like ZHAireS, while reproducing
 232 its results within $\sim 25\%$ error in amplitude [23].

233 3.3. Antenna response

234 In order to compute the voltage generated at the antenna output for
 235 both *microscopic* and *Radio Morphing* methods, we choose in this study the
 236 prototype antenna for the GRAND project: the HORIZONANTENNA [2]. It
 237 is a bow-tie antenna inspired from the *butterfly antenna* [31] developed for
 238 the CODALEMA experiment [32], later used in AERA [33] and adapted to
 239 GRANDProto35 [34]. As for GRANDProto35, three arms are deployed along
 240 the East-West, South-North and vertical axes, but the radiating element is
 241 half its size to better match the 50 – 200 MHz frequency range considered
 242 for GRAND. As the *butterfly antenna*, the HORIZONANTENNA is an active
 243 detector, but in the present study, we simply consider that the radiator is
 244 loaded with a resistor $R = 300\ \Omega$, with a capacitor $C = 6.5 \times 10^{-12}\ \text{F}$ and
 245 inductance $L = 1\ \mu\text{F}$ in parallel. The HORIZONANTENNA is set at an height
 246 of 4.5 m above ground in order to minimize the ground attenuation of the
 247 radio signal.

248 The equivalent length \vec{l}_{eq}^k of one antenna arm k (where $k = \text{EW, NS,}$
 249 Vert) is derived from NEC4 [22] simulations as a function of wave incoming
 250 direction (θ, ϕ) and frequency ν . The voltage at the output of the resistor R
 251 loading the antenna arm is then computed as:

$$252 \quad V^k(t) = \int \vec{l}_{eq}^k(\theta, \phi, \nu) \cdot \vec{E}(\nu) e^{2i\pi\nu t} d\nu \quad (1)$$

253 where $\vec{E}(\nu)$ is the Fourier transform of the radio transient $\vec{E}(t)$ emitted by
 254 the shower.

255 The equivalent length was computed for a vertical antenna deployed over a
 256 flat, infinite ground. The ground slope of the toy setup can then be accounted
 257 for by a simple rotation of this system by an angle α , which translates into
 258 a wave effective zenith angle $\theta^* = \theta - \alpha$, to be used in Eq. 1.

259 3.4. Trigger

260 The last step of the treatment consists in determining whether the shower
 261 could be detected by the radio array. For this purpose, we first apply a
 262 Butterworth filtering of order 5 to the voltage signal in the 50 – 200 MHz
 263 frequency range. This mimics the analog system that would be applied in an
 264 actual setup in order to filter out background emissions outside the designed
 265 frequency range.

266 Then the peak-to-peak amplitude of the voltage V_{pp} is compared to the
 267 level of stationary background noise $\sigma_{\text{noise}} = 15\mu V$, computed as the sum
 268 of Galactic and ground contributions (see [2] and [9] for details). If $V_{\text{pp}} \geq$
 269 $N\sigma_{\text{noise}}$, then we considered that the antenna has triggered. Here $N = 2$
 270 in an aggressive scenario, which could be achieved if innovative triggering
 271 methods [35, 36] were implemented, and $N = 5$ in a conservative one.

272 If at least five antennas trigger on a same shower, then we consider it as
 273 detected.

274 3.5. Cone Model

275 The *Cone Model* proposes to describe the volume inside which the electro-
 276 magnetic radiation is strong enough to be detected as a cone, characterized by
 277 a height and an opening angle varying with shower energy. The *Cone Model*
 278 allows for a purely analytical computation of the radio footprint at ground,
 279 and thus provides a very fast evaluation of the trigger condition, while it
 280 also allows for an easier understanding of the effect of ground topography on
 281 shower detection.

282 The parametrization of the cone height and opening angle as a function of
 283 shower energy needs to be computed once only for a given frequency range.
 284 This was done as follows for the 50 – 200 MHz band considered in this study:

- 285 1. We simulate with the ZHAireS code the electric field from one shower
 286 at different locations set at fixed longitudinal distances L from the
 287 X_{max} position (see Figure 4 for an illustration). Values $L > 100$ km are
 288 not simulated because the maximal value $D = 100$ km chosen in our
 289 study for the distance between the tau decay point and the basis of the
 290 detector (see section 2.4) makes it unnecessary. As the X_{max} position
 291 is reached ~ 15 km after the decay, a distance $L = 100$ km allows to
 292 simulate radio signals over a detector depth of 15 km at least. This is,
 293 in the majority of cases, enough to determine if the shower would be
 294 detected or not.

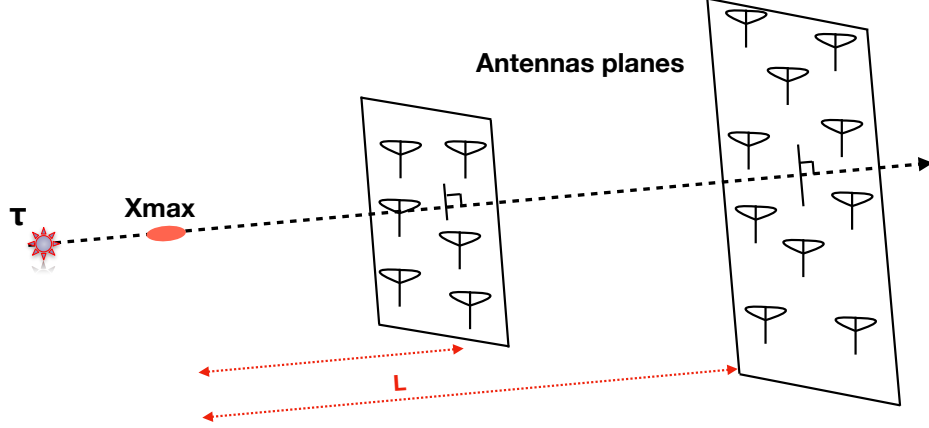


Figure 4: Position of the planes used to parametrize the *Cone Model*. These are placed perpendicular to the shower axis, at various longitudinal distances L from X_{max} . See section 3.5 for details.

2. In each of these antenna planes, identified by an index j in the following, we compute the angular distance between the antennas and the shower core. We determine the maximal angular distance to the shower core Ω^j beyond which the electric field drops below the detection threshold, set to 2 (aggressive) or 5 (conservative) times the value of E_{rms} , the average level of electromagnetic radiation induced by the Galaxy is computed as:

$$E_{\text{rms}}^2 = \frac{Z_0}{2} \int_{\nu_0}^{\nu_1} \int_{2\pi} B_\nu(\theta, \phi, \nu) \sin(\theta) d\theta d\phi d\nu \quad (2)$$

where B_ν is the spectral radiance of the sky, computed with GSM [37] or equivalent codes, $Z_0 = 376.7 \Omega$ the impedance of free space, and $[\nu_0, \nu_1]$ the frequency range considered for detection. Here we choose $\nu_0 = 50$ MHz and $\nu_1 = 200$ MHz, the frequency range of the HORIZO-ANTENNA. The factor $1/2$ arises from the projection of the (unpolarized) Galactic radiation along the antenna axis. We find $E_{\text{rms}} = 22 \mu\text{V/m}$. Defining a detection threshold on the electric field amplitude as done here —rather than the voltage at antenna output as usual— allows to derive results that do not depend on a specific antenna design. It is however not precise: by construction, the details of a specific antenna response and its dependency on the direction of origin of the signal are neglected here, and only the average effect is considered. The

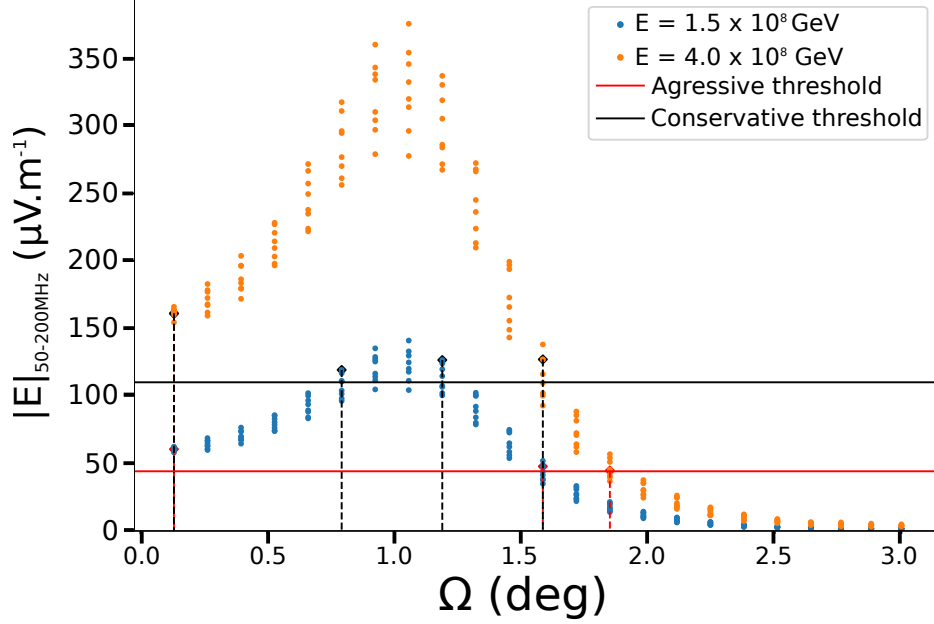


Figure 5: Distribution of the electric field amplitude produced with ZHAireS as a function of Ω , the angular distance to the shower axis, for antennas located at a longitudinal distance of 59 km from X_{\max} . The amplitude dispersion at a given Ω value is due to interplay between Askaryan and geomagnetic effects leading to an azimuthal asymmetry of the signal amplitude. For a shower energy $E = 1.5 \times 10^8$ GeV (in blue) from the $E_\nu = 10^9$ GeV dataset, we find for instance $(\Omega_{\min}^j; \Omega_{\max}^j) = (0.1^\circ; 1.7^\circ)$ in the aggressive case and $(0.8^\circ; 1.2^\circ)$ in the conservative one.

Cone Model is therefore only an approximate method.

The distribution of the electric field amplitudes as a function of the angular distance to the shower axis is shown for illustration in Figure 5 for the plane j located at a longitudinal distance $L = 59$ km. As the Cherenkov ring induces an enhancement in the amplitude profile for $\Omega \sim 1^\circ$, we actually compute two values of the angle Ω^j : Ω_{\min}^j and Ω_{\max}^j , thus defining the angular range inside which the electric field amplitude is above the detection threshold.

3. The value of Ω^j does not vary significantly with L (see Figure 6). This validates the choice of a conical model for the trigger volume and allows to derive a single set of values $(\Omega_{\min}; \Omega_{\max}) = (\langle \Omega_{\min}^j \rangle; \langle \Omega_{\max}^j \rangle)$ for one

- specific energy.
4. A similar procedure is applied to determine the cone height H , set to be equal to the longitudinal distance L up to which the signal is strong enough to be detected.

Table 1: Parameters for the fitting functions given in Equations 3 and 4, for aggressive and conservative thresholds and maximal and minimum Ω angles. Parameters a and b are in km, c and d in degrees.

threshold	a	b	Ω	c	d
aggressive	109 ± 15	116 ± 3	min	0.20 ± 0.02	-2.4 ± 0.2
			max	1.3 ± 0.2	1.00 ± 0.02
conservative	42 ± 7	48 ± 1	min	1.2 ± 0.2	-2.2 ± 0.2
			max	1.0 ± 0.3	0.80 ± 0.03

5. We repeat the treatment for various shower energies E_{sh} by rescaling the signals amplitudes and thus obtain the distributions $\Omega(E_{\text{sh}})$ and $H(E_{\text{sh}})$ shown in Figures 7 and 8. We fit these distributions for shower energies larger than $3 \cdot 10^7$ GeV with analytic functions given by

$$H|_{50-200\text{MHz}} = a + b \left(\frac{E_{\text{sh}} - 10^{17}\text{eV}}{10^{17}\text{eV}} \right), \quad (3)$$

$$\Omega|_{50-200\text{MHz}} = c + d \log \left(\frac{E_{\text{sh}}}{10^{17}\text{eV}} \right). \quad (4)$$

with E_{sh} expressed in eV in the formulas. Numerical values of a, b, c, d are given in Table 1.

The three parameters Ω_{min} , Ω_{max} and H allow to define a hollow cone, with an apex set at the shower X_{max} location and oriented along the shower axis. Any antenna located inside this volume is supposed to trigger on the shower according to the *Cone Model*.

As mentioned in the introduction, the interplay between the geomagnetic effect and the charge excess induces an asymmetry on the electric field amplitude as a function of antenna angular position w.r.t. the shower core. This can be seen on Figure 5, for instance, where the dispersion in field strength at a given angular distance is the exact illustration of this phenomenon. The *Cone Model* however assumes a rotation symmetry around the shower axis and thus neglects this asymmetry. This is still acceptable if we are only interested in the average

number of triggered antennas by the shower —which is the case here—
and not in the amplitude pattern of the radio signal.

Once this parametrization is completed, the *Cone Model* is applied to the
selected set of tau decays: the values of the cone parameters are computed
for the energy and geometry of each shower and the intersection between the
resulting cone volume and the detection area is calculated. If at least five
antennas fall within this intersection, then we consider that the shower is
detected.

4. Results

We have computed the detection efficiency for our toy setup through the
three independent simulation chains presented in section 2. Detection effi-
ciency is defined here as the ratio of the number of showers detected to the
total of 100 selected tau decays. The parameters ranges explored initially are
distances $D = \{20, 30, 40, 60, 80, 100\}$ km and slopes $\alpha = \{0, 5, 10, 15, 20, 45, 90\}$
degrees. This coarse step is mainly motivated by computation time and disk
space considerations for the *microscopic* simulation.

We first show a relative comparison of the different methods before dis-
cussing the effects of the topography on the detection efficiency.

4.1. Relative comparison

Figure 9 shows that the *Radio Morphing* treatment induces trigger ef-
ficiencies at most 15% higher than *microscopic* simulations. This confirms
results obtained in [23] and qualifies the *Radio Morphing* chain as a valid
tool for the study presented in this article. Taking advantage of the factor
 ~ 100 gain in computation time of *Radio Morphing* compared to *microscopic*
simulations [23] we then decrease the simulation step size down to 2° for slope
 α and 5 km for the distance to decay D , allowing for a more detailed study
of the effect of topography on the array detection efficiency.

This refined analysis is presented in Figure 10, where results of the *Cone*
Model are also shown. The distribution of the *Cone Model* detection efficiency
in the (α, D) plane follows a trend similar to the *Radio Morphing* one, with
differences within $\pm 20\%$ for most of the parameter space (α, D) . There
are however some differences, in particular a significant under-estimation
with the *Cone Model* in the ranges $(\alpha > 30^\circ, D > 80 \text{ km})$ and $(\alpha < 20^\circ,$
 $D < 30 \text{ km})$. There is also a flatter distribution as a function of slope for

384 the conservative trigger hypothesis, which results in an over-estimation for
 385 ($\alpha > 30^\circ$, $D < 40$ km) for the *Cone Model*, also visible on Figure 11.

386 Discrepancies are not surprising since the *Cone Model* is an approximate
 387 method as already pointed out in section 3.5. One should however be re-
 388 minded that slopes $\alpha > 30^\circ$ correspond to extreme cases, very rare in reality
 389 and which cannot be considered for actual deployment. For realistic slope
 390 values $\alpha < 30^\circ$, the *Cone Model* detection efficiencies differ from those of
 391 the *microscopic* approach by -30% at most. The *Cone Model* can thus safely
 392 be used to provide in a very short amount of time a rough and conservative
 393 estimate of the neutrino sensitivity for realistic topographies. This result
 394 also provides an *a posteriori* validation of the initial computation of the
 395 GRAND array sensitivity [24], even though the cone was then parametrized
 396 from showers simulated in the 30-80 MHz frequency range.

397 4.2. Toy-setup discussion

398 Below we study how the topography affects the detection potential of
 399 neutrino-induced air showers by a radio array. To do that, we use the results
 400 of the *Radio Morphing* chain, which provide at the same time good reliability
 401 and fine topography granularity as explained in the previous section.

402 Despite statistical fluctuations obviously visible in Figures 10 and 11,
 403 general trends clearly appear. Four striking features can in particular be
 404 singled-out:

- 405 • A significant increase of the detection efficiency for slopes varying from 0
 406 degree up to few degrees: the detection efficiency for a flat area is lower by
 407 a factor 3 compared to an optimal configuration $(\alpha, D) \approx (10^\circ, 25 \text{ km})$. This
 408 result is consistent with the study presented in [2], where the effective area
 409 computed for a real topography on a mountainous site was found to be four
 410 times larger than for a flat site.
- 411 • Limited variation of the detection efficiency for slopes between $\sim 2^\circ$ and
 412 $\sim 20^\circ$.
- 413 • An efficiency slowly decreasing for slopes larger than $\sim 20^\circ$. This is in
 414 particular valid for distances D shorter than 40 km, where the detection
 415 efficiency is nearly null.
- 416 • A slow decrease of the detection efficiency with increasing value of D .

417 To interpret these results, we may first consider that two conditions have
 418 to be fulfilled to perform radio-detection of showers: first the radio beam must
 419 hit the detector, then enough antennas (five in this study) have to trigger

on the corresponding radio signal. In order to disentangle these two factors —one mostly geometrical, the other experimental—, we display in Figure 12 the fraction of events reaching the detector as a function of the parameters (α, D) . These events are defined by a non-null intersection between the detector plane and a 3° half-aperture cone centered on the shower trajectory, a conservative and model-independent criterion.

It appears from Figure 12 that the large fraction —around 90%— of showers flying above the detector is the main cause of the limited efficiency of a flat detection area. As a corollary, the steep rise of detection efficiency with increasing slope is clearly due to the increasing fraction of intercepted showers. Figures 10 and 12 however differ significantly for configurations corresponding to $\alpha > 20^\circ$ and $D < 40$ km: the fraction of intercepted events varies marginally with α at a given D , while the detection efficiency drops. This means that the first condition for detection —detector inside the radio beam— is fulfilled for these configurations, but the second —sufficient number of triggered antennas— is not, because the tau decay is too close, and the radio footprint at ground consequently too small. The situation may be compared —with a 90° rotation of the geometry of the problem— to the radio-detection of "standard" air showers with zenith angle $\theta < 60^\circ$, which suffers from limited efficiency for sparse array [9]. A larger density of detection units would certainly improve detection efficiency, but the need for large detection areas, imposed by the very low rate of neutrino events, discards this option.

Finally the slow decrease in efficiency with increasing value of D is mostly due to geometry, as the fraction of intersecting events diminishes with D in similar proportion.

Yet, one could argue that this result is biased by the detector layout defined in our toy-setup. The infinite width of the detection plane combined with a limit on the detector elevation (3000 m above the reference altitude, see section 2.4) indeed implies that a detector deployed over mild slopes is larger than one deployed over steeper ones in this study. A value $\alpha = 10^\circ$ for example allows for a detector extension of $3/\sin \alpha \sim 17$ km, while $\alpha = 70^\circ$ implies a value six times smaller. Considering a constant detector area for all configurations (α, D) and comparing their effective area —or expected event rates— would avoid such bias, but would require a complete Monte-Carlo simulation. This is beyond the scope of this study, and would be useful only if real topographies were taken into account.

457 It is however possible to estimate this bias by studying how the *constant*
458 *area detector efficiency* varies with slope. This quantity is defined as the
459 detection efficiency averaged over D and weighted with a factor $\sin \alpha$. As D
460 measures the amount of empty space in front of the detector (see section 2.4),
461 averaging the efficiency over all values of D allows us to take into account all
462 possible shower trajectories for a given slope value. The factor $\sin \alpha$ corrects
463 for the variation of the detector area with slope. The *constant area detector*
464 *efficiency* can therefore be understood as a proxy for the event rate per unit
465 area of a detector deployed on a plane of slope α , facing an infinite flat area.
466 The *constant area average efficiency* computed from the *Radio Morphing*
467 results is displayed as a function of slope on Figure 13.

468 Beyond a certain threshold ($\sim 20^\circ$ for the conservative case, $\sim 30^\circ$ for the
469 aggressive one), there is no significant variation of its value with α , because
470 the poor performance of steep slopes for close-by showers (i.e. small values
471 of D) compensates for the larger area factor $\sin \alpha$. Figure 13 also confirms
472 the clear gain of a slope—even mild—compared to a detector deployed over
473 flat ground.

474 Only showers propagating towards the slope were considered in this study,
475 but one can deduce from Figures 11 and 12 that the opposite trajectory
476 (corresponding to a down-going slope, i.e. $\alpha < 0$) results in a ~ 0 detection
477 probability. For showers traveling transverse to the slope inclination (i.e.
478 along the East-West axis in our configuration), basic geometric considerations
479 allow to infer that the situation is probably comparable to horizontal ground.
480 The boost effect of value 3 determined for showers propagating towards the
481 detector plane thus certainly corresponds to a best-case scenario. Computing
482 the net effect of a non-flat topography on the neutrino detection efficiency
483 for random direction of arrivals cannot be performed with this toy-setup
484 configuration (see section 2.4 for details). However we note that a study
485 presented in Ref. [2] points towards a boost factor of ~ 2 on the detection of
486 upward-going showers for the specific site used in that work.

487 5. Conclusion

488 We have studied the impact of the topography for radio-detection of
489 neutrino-induced Earth-skimming air showers. For this purpose, we have
490 developed a toy setup with a simplified topography for the detector, depend-
491 ing on two parameters: the distance between the air shower injection point
492 and the detector array, and the ground slope of the detector array. We have

493 computed the neutrino detection efficiency of this toy detector configuration
 494 through three computation chains: a microscopic simulation of the shower
 495 development and its associated radio emission, a radio-signal computation
 496 using *Radio Morphing* and an analytical treatment based on a *cone model* of
 497 the trigger volume.

498 The comparison of these three independent tools confirms that *Radio*
 499 *Morphing* is a reliable method in this framework, while the *Cone Model* offers
 500 a fast, conservative estimate of the detection efficiency for realistic topogra-
 501 phies. The latter can thus be used to perform in a negligible amount of time
 502 a preliminary estimate of the potential for neutrino detection of a given zone,
 503 and the former can then be used to carry out a detailed evaluation of selected
 504 sites instead of full Monte-Carlo simulations.

505 More importantly, the results presented here show that ground topog-
 506 raphy has a great impact on the detection efficiency, with an increase by a
 507 factor ~ 3 for angles of just a few degrees compared to a flat array [and for an](#)
 508 [optimal case where shower trajectories face the detector plane](#). This boost
 509 effect is very similar for any slope value ranging between 2° and 20° . The
 510 other noticeable result of this study is the moderate effect of the distance on
 511 the detection efficiency, with comparable values for tau decays taking place
 512 between 20 and 100 km from the detector.

513 [Two slopes facing each other with tens of kilometers between them may](#)
 514 [therefore constitute the optimal configuration for neutrino detection, as they](#)
 515 [would correspond to enhanced rates for the two directions perpendicular to](#)
 516 [the slopes. Wide valleys or large basins could offer such topographies](#) and
 517 will consequently be primarily targeted in the search for the optimal sites
 518 where the $\mathcal{O}(10)$ sub-arrays composing the GRAND array could be deployed
 519 to optimize its neutrino detection efficiency. An effort in this direction has
 520 been initiated in the framework of the GRAND project.

521 *Acknowledgments*

522 We are grateful to Clementina Medina and Jean-Christophe Hamilton
 523 for suggesting this study. This work is supported by the APACHE grant
 524 (ANR-16-CE31-0001) of the French Agence Nationale de la Recherche. We
 525 also thank the France China Particle Physics Laboratory for its support.
 526 The simulations were performed using the computing resources at the CC-
 527 IN2P3 Computing Centre (Lyon/Villeurbanne France), partnership between
 528 CNRS/IN2P3 and CEA/DSM/Irfu.

6. References

- [1] K. Fang, K. Kotera, M. C. Miller, K. Murase, F. Oikonomou, Identifying ultrahigh-energy cosmic-ray accelerators with future ultrahigh-energy neutrino detectors, *JCAP* 12 (2016) 017. arXiv:1609.08027, doi:10.1088/1475-7516/2016/12/017.
- [2] J. Alvarez-Muñiz, et al., The Giant Radio Array for Neutrino Detection (GRAND): Science and Design, *Sci. China Phys. Mech. Astron.* 63 (1) (2020) 219501. arXiv:1810.09994, doi:10.1007/s11433-018-9385-7.
- [3] D. Fargion, A. Aiello, R. Conversano, Horizontal tau air showers from mountains in deep valley: Traces of uhecr neutrino tau, in: *Proceedings, 26th International Cosmic Ray Conference, August 17-25, 1999, Salt Lake City: Invited, Rapporteur, and Highlight Papers, 1999*, p. 396, [2,396(1999)]. arXiv:astro-ph/9906450.
- [4] H. Falcke, et al., Detection and imaging of atmospheric radio flashes from cosmic ray air showers, *Nature* 435 (2005) 313–316. arXiv:astro-ph/0505383, doi:10.1038/nature03614.
- [5] D. Ardouin, et al., Geomagnetic origin of the radio emission from cosmic ray induced air showers observed by CODALEMA, *Astropart. Phys.* 31 (2009) 192–200. arXiv:0901.4502, doi:10.1016/j.astropartphys.2009.01.001.
- [6] P. A. Bezyazeev, et al., Measurement of cosmic-ray air showers with the Tunka Radio Extension (Tunka-Rex), *Nucl. Instrum. Meth. A* 802 (2015) 89–96. arXiv:1509.08624, doi:10.1016/j.nima.2015.08.061.
- [7] A. Aab, et al., Energy Estimation of Cosmic Rays with the Engineering Radio Array of the Pierre Auger Observatory, *Phys. Rev. D* 93 (12) (2016) 122005. arXiv:1508.04267, doi:10.1103/PhysRevD.93.122005.
- [8] S. Buitink, et al., A large light-mass component of cosmic rays at $10^{17} - 10^{17.5}$ eV from radio observations, *Nature* 531 (2016) 70. arXiv:1603.01594, doi:10.1038/nature16976.
- [9] D. Charrier, et al., Autonomous radio detection of air showers with the TREND50 antenna array, *Astropart. Phys.* 110 (2019) 15–29. arXiv:1810.03070, doi:10.1016/j.astropartphys.2019.03.002.

- [10] D. Ardouin, et al., First detection of extensive air showers by the TREND self-triggering radio experiment, *Astropart. Phys.* 34 (2011) 717–731. arXiv:1007.4359, doi:10.1016/j.astropartphys.2011.01.002.
- [11] G. Askaryan, Excess negative charge of an electron-photon shower and its coherent radio emission, *Sov. Phys. JETP* 14, 441 (1962).
- [12] G. Askaryan, Coherent radio emission from cosmic showers in air and in dense media, *Sov. Phys. JETP* 21, 658 (1965).
- [13] F. D. Kahn, I. Lerche, A. C. B. Lovell, Radiation from cosmic ray air showers, *P. Roy. Soc. A - Math. Phys.* A-289 (1966) 206.
- [14] O. Scholten, K. Werner, F. Rusydi, A macroscopic description of coherent geo-magnetic radiation from cosmic-ray air showers, *Astropart. Phys.* 29 (2008) 94–103. arXiv:0709.2872, doi:10.1016/j.astropartphys.2007.11.012.
- [15] T. Huege, Radio detection of cosmic ray air showers in the digital era, *Phys. Rept.* 620 (2016) 1–52. arXiv:1601.07426, doi:10.1016/j.physrep.2016.02.001.
- [16] F. G. Schröder, Radio detection of Cosmic-Ray Air Showers and High-Energy Neutrinos, *Prog. Part. Nucl. Phys.* 93 (2017) 1–68. arXiv:1607.08781, doi:10.1016/j.ppnp.2016.12.002.
- [17] J. Alvarez-Muñiz, W. R. Carvalho, D. García-Fernández, H. Schoorlemmer, E. Zas, Simulations of reflected radio signals from cosmic ray induced air showers, *Astropart. Phys.* 66 (2015) 31–38. arXiv:1502.02117, doi:10.1016/j.astropartphys.2014.12.005.
- [18] A. Aab, et al., Observation of inclined EeV air showers with the radio detector of the Pierre Auger Observatory, *JCAP* 1810 (10) (2018) 026. arXiv:1806.05386, doi:10.1088/1475-7516/2018/10/026.
- [19] V. Niess, O. Martineau-Huynh, DANTON: a Monte-Carlo sampler of τ from ν_τ interacting with the Earth (2018). arXiv:1810.01978.
- [20] V. Niess, Danton: Decaying taus from neutrinos, GitHub repository (2017–2018).
URL <https://github.com/niess/danton>

- [21] J. Alvarez-Muñiz, W. R. Carvalho, E. Zas, Monte Carlo simulations of radio pulses in atmospheric showers using ZHAireS, *Astropart. Phys.* 35 (2012) 325–341. arXiv:1107.1189, doi:10.1016/j.astropartphys.2011.10.005.
- [22] G. Burke, Numerical Electromagnetics Code – NEC-4, Method of Moments, Part I: User’s Manual, Lawrence Livermore National Lab., Rept. URCL-MA-109338 Pt. I (1992).
URL http://physics.princeton.edu/~mcdonald/examples/NEC_Manuals/NEC4UsersMan.pdf
- [23] A. Zilles, O. Martineau-Huynh, K. Kotera, M. Tueros, K. de Vries, W. Carvalho Jr., V. Niess, N. Renault-Tinacci, V. Decoene, Radio Morphing: towards a fast computation of the radio signal from air showers, *Astropart. Phys.* 114 (2020) 10–21. arXiv:1811.01750, doi:10.1016/j.astropartphys.2019.06.001.
- [24] O. Martineau, K. Kotera, K. Fang, Z. Feng, C. Finley, Q. Gou, V. Niess, N. Renault-Tinacci, C. Timmermans, D. Charrier, S. de Jong, K. de Vries, J. Gu, H. HU, K. Murase, F. Oikonomou, J. Schmid, Z. Wang, X. Wu, J. Zhang, Y. Zhang, The Giant Radio Array for Neutrino Detection, in: *Proceedings of The 34th International Cosmic Ray Conference — PoS(ICRC2015)*, Vol. 236, 2016, p. 1143. doi:10.22323/1.236.1143.
- [25] J. Alvarez-Muñiz, W. R. Carvalho, K. Payet, A. Romero-Wolf, H. Schoorlemmer, E. Zas, Comprehensive approach to tau-lepton production by high-energy tau neutrinos propagating through the Earth, *Phys. Rev. D* 97 (2) (2018) 023021. arXiv:1707.00334, doi:10.1103/PhysRevD.97.023021.
- [26] V. Niess, A. Barnoud, C. Cârloganu, O. Martineau-Huynh, TURTLE: A C library for an optimistic stepping through a topography (2019). arXiv:1904.03435, doi:10.1016/j.cpc.2019.106952.
- [27] A. M. Dziewonski, D. L. Anderson, Preliminary reference earth model, *Physics of the Earth and Planetary Interiors* 25 (4) (1981) 297 – 356. doi:[https://doi.org/10.1016/0031-9201\(81\)90046-7](https://doi.org/10.1016/0031-9201(81)90046-7).

- [28] See the following link to the pdg for a discussion about standard rock.
URL <http://pdg.lbl.gov/2015/AtomicNuclearProperties/standardrock.html>
- [29] E. Zas, F. Halzen, T. Stanev, Electromagnetic pulses from high-energy showers: Implications for neutrino detection, *Phys. Rev. D* 45 (1992) 362–376. doi:10.1103/PhysRevD.45.362.
- [30] S. J. Sciutto, AIRES: A system for air shower simulations (1999). arXiv:astro-ph/9911331, doi:10.13140/RG.2.2.12566.40002.
- [31] D. Charrier, CODALEMA Collaboration, Antenna development for astroparticle and radioastronomy experiments, *Nucl. Instrum. Meth. A* 662 (2012) S142–S145. doi:10.1016/j.nima.2010.10.141.
- [32] A. Escudie, D. Charrier, R. Dallier, D. Garca-Fernandez, a. lecacheux, L. Martin, B. Revenu, From the Observation of UHECR Radio Signal in [1-200] MHz to the Composition: CODALEMA and EXTASIS Status Report, *PoS ICRC2019* (2019) 246. doi:10.22323/1.358.0246.
- [33] P. Abreu, et al., Antennas for the detection of radio emission pulses from cosmic-ray, *JINST* 7 (2012) P10011. arXiv:1209.3840, doi:10.1088/1748-0221/7/10/P10011.
- [34] Q. Gou, et al., The GRANDproto35 experiment, *PoS ICRC2017* (2018) 388. doi:10.22323/1.301.0388.
- [35] F. Fühner, T. Charnock, A. Zilles, M. Tueros, Towards online triggering for the radio detection of air showers using deep neural networks, in: *Proceedings, Acoustic and Radio EeV Neutrino Detection Activities (ARENA 2018): Catania, Italy, June 12-15, 2018, Vol. 216, 2019, p. 03004*. arXiv:1809.01934, doi:10.1051/epjconf/201921603004.
- [36] M. Erdmann, F. Schlter, R. Smida, Classification and Recovery of Radio Signals from Cosmic Ray Induced Air Showers with Deep Learning, *JINST* 14 (04) (2019) P04005. arXiv:1901.04079, doi:10.1088/1748-0221/14/04/P04005.
- [37] H. Zheng, et al., An improved model of diffuse galactic radio emission from 10 MHz to 5 THz, *Mon. Not. Roy. Astron. Soc.* 464 (3) (2017) 3486–3497. arXiv:1605.04920, doi:10.1093/mnras/stw2525.

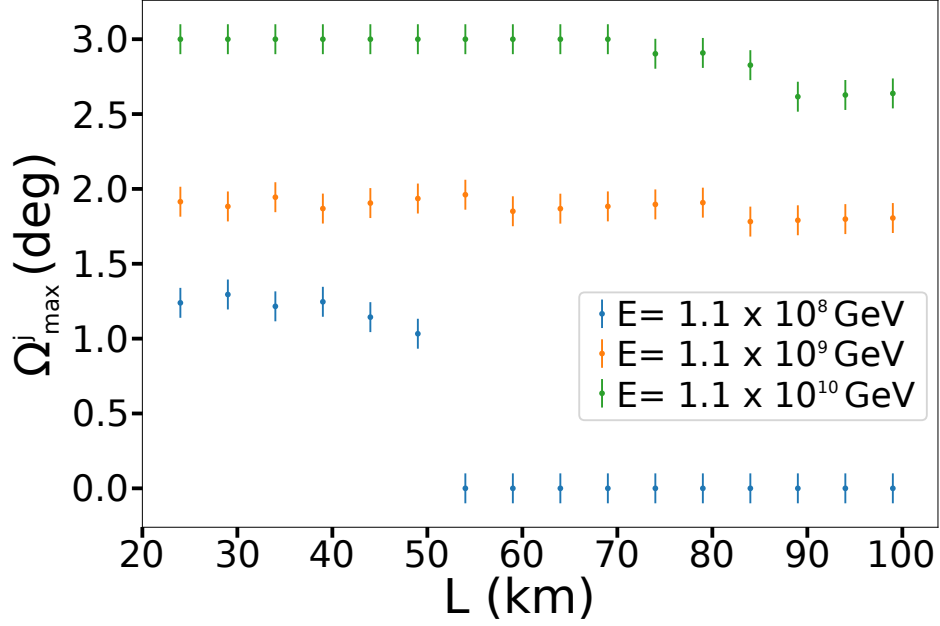


Figure 6: Angular distances Ω_{\max}^j computed following the method presented in Figure 5 as a function of longitudinal distance for various shower energies. Ω_{\max} measures the maximum opening angle of the cone describing the triggering volume, while index j identifies the simulation plane perpendicular to the shower axis (see Figure 4). Here only the conservative case is shown.

The angle value varies marginally over the full range of longitudinal values considered for shower energies $E = 1.1 \times 10^9$ and 1.1×10^{10} GeV, validating the choice of a cone model —with fixed opening angle $\Omega_{\max} = \langle \Omega_{\max}^j \rangle$ — for the trigger volume modeling. For $E = 1.1 \times 10^8$ GeV, Ω drops to 0 for $L > 50$ km because the cone height H is equal to 50 km in the conservative case (see Figure 8). Similar treatment is applied to determine Ω_{\min} .

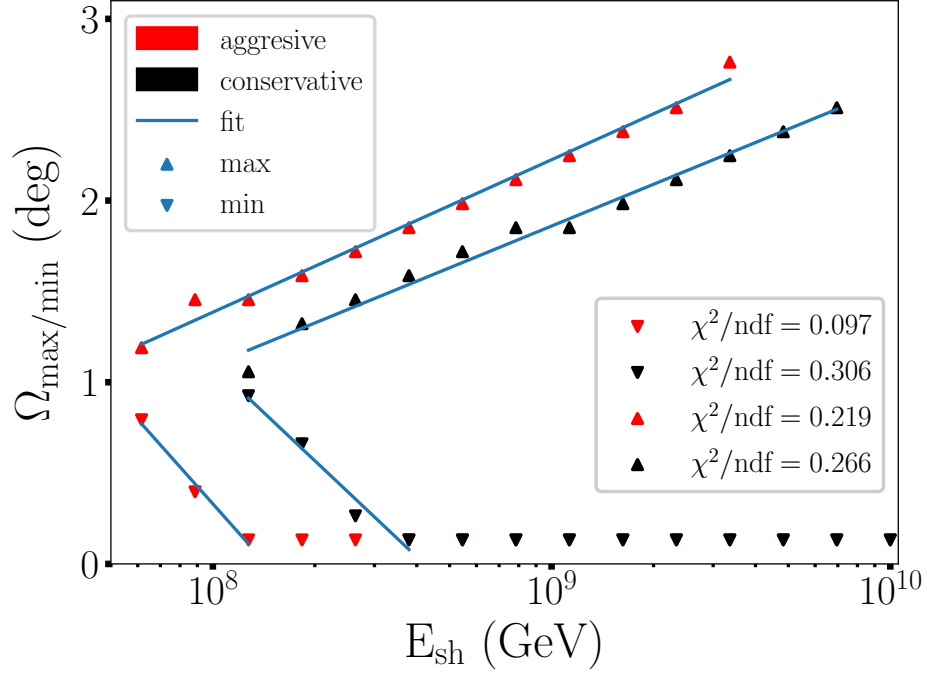


Figure 7: Angles Ω_{\max} and Ω_{\min} as a function of shower energy E_{sh} ; and fit by Eq. 4. Angles Ω_{\max} and Ω_{\min} define the inner and outer boundaries of the hollow cone and are obtained by averaging the values Ω_{\max}^j and Ω_{\min}^j (see Figure 6)

. At the highest energies, Ω_{\min} drops down to 0° , implying that the radio signal is above the detection threshold for all angular distances $\Omega \leq \Omega_{\max}$.

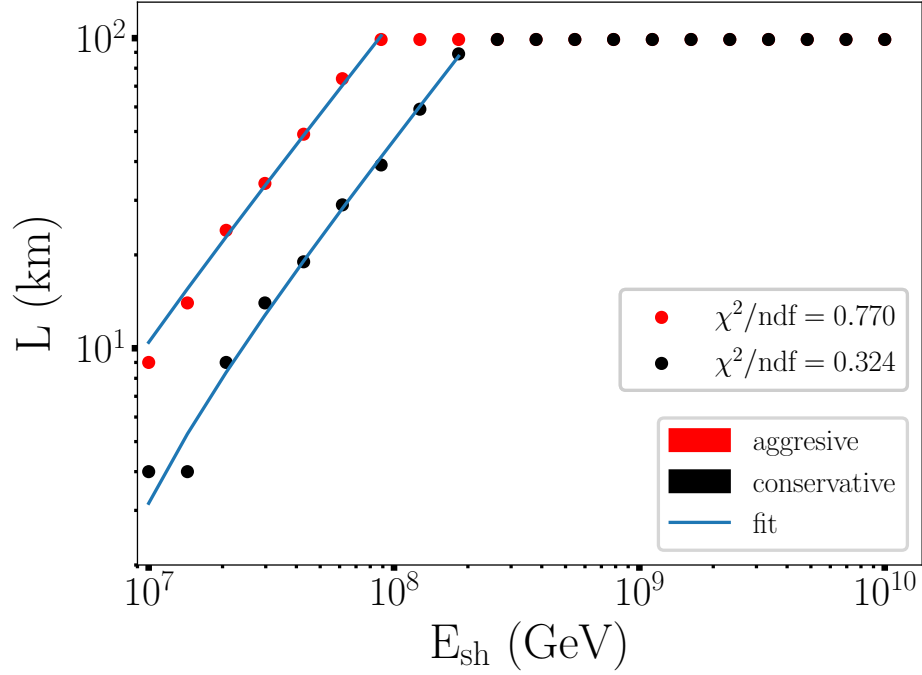


Figure 8: Cone height H as a function of shower energy E_{sh} and fit by Eq. 3. Cone height saturates at values $H = 100$ km, because the antenna planes used to parametrize the *Cone Model* do not extend beyond this value. However points with values $H < 100$ km suffice to demonstrate that the cone heights scale linearly with energy, as one would naturally expect, since the electric field amplitude also scales linearly with energy. Cone height values $H > 100$ km are therefore extrapolated from the fit given in Eq. 3.

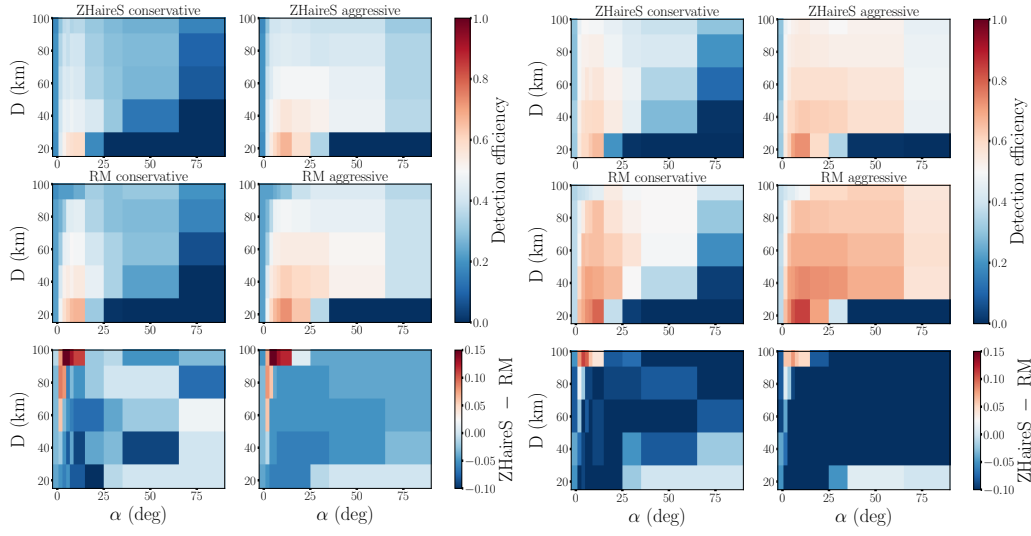


Figure 9: *Left*: Detection efficiency as a function of the distance D and slope α for the simulation set with a primary neutrino energy of 10^9 GeV. Comparison between ZHAireS and *Radio Morphing* (respectively *top* and *middle* plots, while the difference is plotted at the *bottom*) and conservative thresholds (*left*) and aggressive thresholds (*right*). *Right*: Same for a primary neutrino energy of 10^{10} GeV.

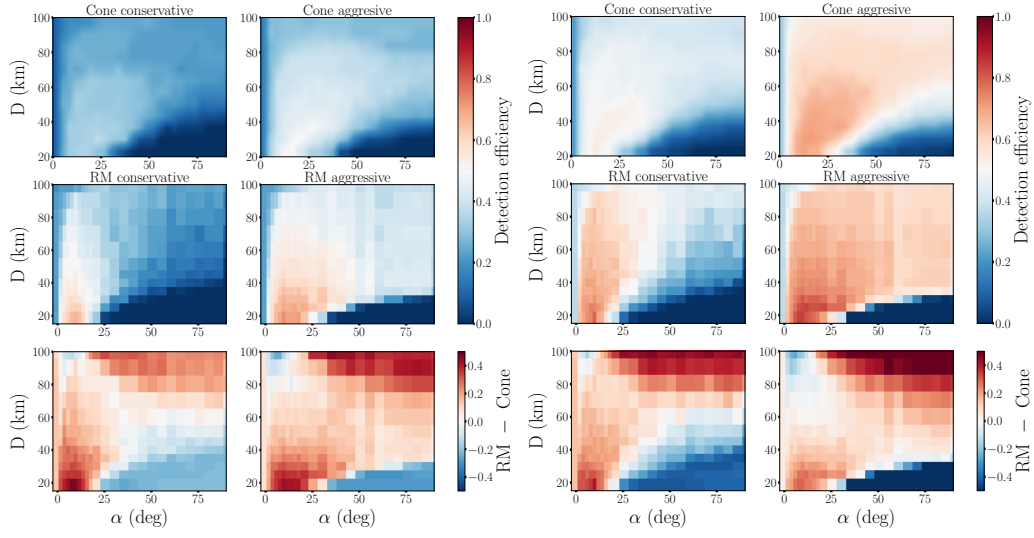


Figure 10: *Left:* Detection efficiency as a function of distance D and slope α for the simulation set with a primary neutrino energy of 10^9 GeV. Results are plotted for the *Cone Model* (top) and *Radio Morphing* (middle), as well as the difference (*Radio-Morphing* - *Cone Model*) (bottom). Conservative (left) and aggressive (right) threshold hypothesis are also considered (right). *Right:* Same for a primary neutrino energy of 10^{10} GeV.

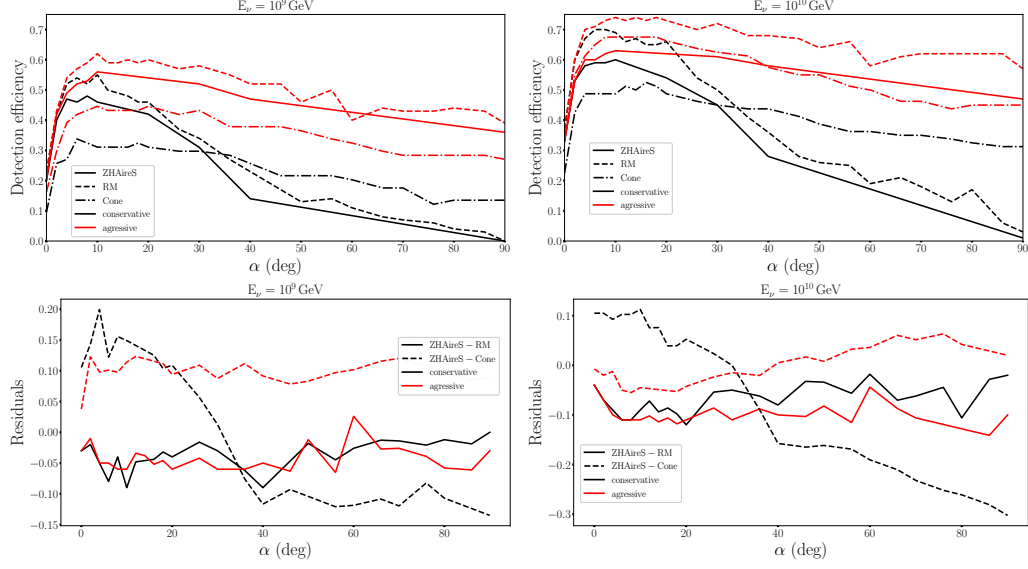


Figure 11: *Top*: Detection efficiency as a function of slope α for a distance $D = 40$ km for neutrinos energies of 10^9 (left) and 10^{10} GeV (right). Comparisons between the microscopic (solid lines), *Radio Morphing* (dashed lines) and *Cone Model* (dash-dotted lines), for conservative (black lines) and aggressive (red lines) threshold hypothesis. *Bottom*: Differences *ZHAireS*-*RadioMorphing* and *ZHAireS* - *Cone Model* for the data shown in the top panel, following the same color code.

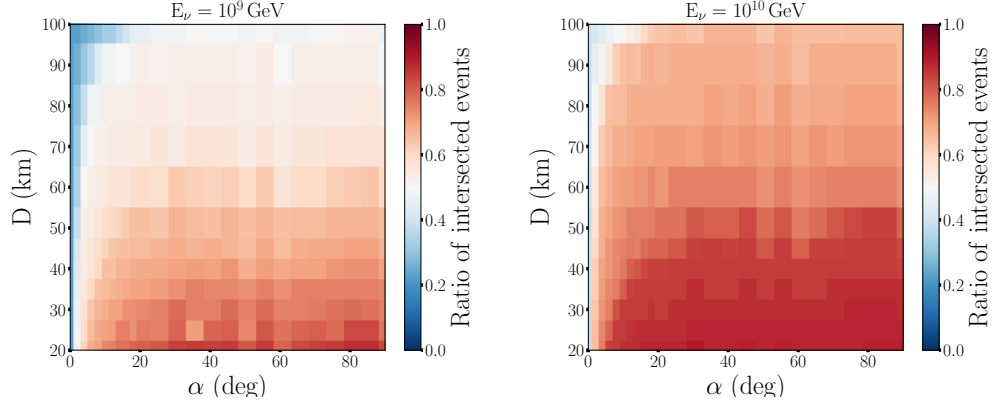


Figure 12: *Left*: Fraction of events intersecting the detection area as a function of distance D and slope α for the simulation set with a primary neutrino energy of 10^9 GeV. *Right*: Same for a primary neutrino energy of 10^{10} GeV.

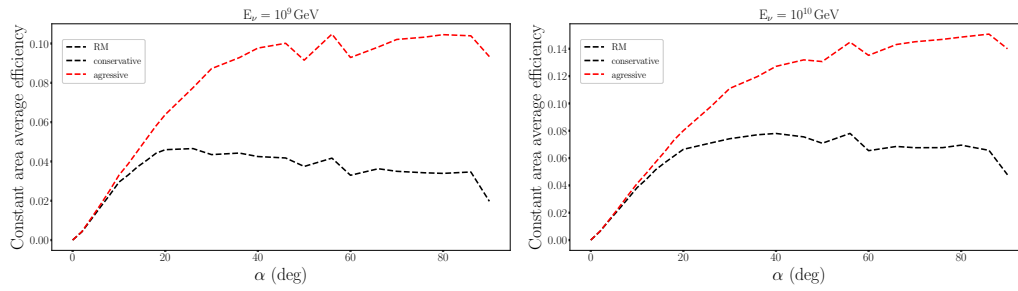


Figure 13: *Left:* Average detection efficiency over a constant detector area as a function of slope for the simulation set with a primary neutrino energy of 10^9 GeV. *Right:* Same for a primary neutrino energy of 10^{10} GeV. In both cases values are computed with the *Radio Morphing* treatment.